



PERGAMON

Available online at www.sciencedirect.com

SCIENCE @ DIRECT®

Chaos, Solitons and Fractals 19 (2004) 1087–1094

CHAOS
SOLITONS & FRACTALS

www.elsevier.com/locate/chaos

Folding characterization in conservative chaotic fluid flows

Fábio H. Palladino^{a,*}, Gilberto Corso^b, Iberê L. Caldas^a

^a *Instituto de Física, Universidade de São Paulo, Caixa Postal 66318, 05315-970 São Paulo, SP, Brazil*

^b *Departamento de Física Teórica e Experimental, Universidade Federal do Rio Grande do Norte, 59078-970 Natal, RN, Brazil*

Accepted 29 May 2003

Abstract

We study transport of passive scalar fields in a bidimensional incompressible chaotic fluid flow. For a spatially smooth velocity field with impulsive perturbations, the model is described by a randomized standard mapping. We numerically investigate passive scalar field transport for given initial concentration distributions and their dependence on the nonlinearity and noise amplitude. We show that space and time concentration histograms are determined by the underlying mechanism of stretching and folding. Moreover, to characterize this process we introduce a parameter, the average derivative of a tracer line length, which shows interesting scale properties.

© 2003 Elsevier Ltd. All rights reserved.

1. Introduction

Several recent experiments in fluids have provided detailed measurements for the passive transport of scalar quantities such as impurity concentration. This transport leads to mixing in fluids that are not necessarily turbulent. These processes seem to be connected to chaotic dynamics of the streamlines and have been observed even for simple velocity fields in laminar flows [1–5].

To investigate the evolution of scalar quantities or contaminants when the fluid element trajectories are chaotic, several two-dimensional, time-periodic flow fields generating chaotic streamlines have been proposed in the literature [6–11]. In these models the physical mechanism of mixing is a consequence of streamline diffusion, which creates smaller and smaller length scales of the scalar field by successive stretching and folding. Complementarily, these models have been extended to simulate fluid turbulence, which homogenizes the local gradients observed in the scalar field. This has been achieved by introducing a randomic perturbation to phase angles of the deterministic flows. Then, a Lagrangian approach have been adopted, requiring the computation of a large number of particle trajectories and global characterization of the scalar field at large time [12–15].

Motivated by the problem of passive transport in a confined fluid, we study a dynamical system that describes mixing. In particular, we consider the enhancement of streamline diffusion due to the Lagrangian chaos of the velocity field lines perturbed by a sequence of periodic kicks. For that, we use a conservative phenomenological model, introduced in Ref. [12], for which the field line diffusion is described by the standard map [2,16] with a perturbing randomic phase. In this model mixing is not derived from the fluid dynamic equations but from the velocity flow. The prescribed flow is chaotic, meaning that nearby fluid elements diverge exponentially with time. According to the model, a small amount of dye or other kind of contaminant is transported by the fluid without otherwise influencing the fluid motion, thus acting as a passive tracer of the fluid flow. Turbulence is not intrinsic since there is no dissipation assumption, but it is simulated by the presence of a randomic phase that introduces flux instabilities. We will see that this artifice does not affect the area preserving properties of the model.

* Corresponding author.

We provide a numerical evidence of randomized concentration distribution in the model and verify a simple direct relation between time and space series histograms and the initial contaminant distribution. To characterize general transport features we define a numerical parameter that measures tracer line deformation on time and show its dependence on the model parameter that characterizes nonlinearity. The deformation parameter is directly related to the line folding and constitutes an original way to characterize folding in chaotic fluxes. With the parameter introduced in this work, we verify a behavior we expect to observe in other chaotic conservative fluxes.

The paper is organized as follows: in Section 2 the flux model is introduced; in Section 3 we analyse contaminant distributions; in Section 4 we characterize folding features and in Section 5 the conclusions are given.

2. The model

In this section we introduce the bidimensional fluid model we examine, based on standard map. The scalar field Φ describing a passive contaminant concentration is supposed to evolve according to a incompressible law

$$\frac{d\Phi}{dt} = \frac{\partial\Phi}{\partial t} + \mathbf{v} \cdot \nabla\Phi = 0, \quad (1)$$

where $\mathbf{v} \equiv d\mathbf{r}/dt$ is the velocity vector of a fluid element on position \mathbf{r} at time t .

We follow Ref. [12] concerning the particular bidimensional field $\mathbf{v}(\mathbf{r}, t)$ given by

$$\mathbf{v}(\mathbf{r}, t) = v_1 y \hat{\mathbf{x}} + v_2 \sin[\theta(t) + x] \delta_T(t) \hat{\mathbf{y}}, \quad (2)$$

where

$$\delta_T(t) = T \sum_{n=-\infty}^{\infty} \delta(t - nT) \quad (3)$$

is a periodic impulse function, $\hat{\mathbf{x}}$ and $\hat{\mathbf{y}}$ are the unitary vectors in the x and y directions and v_1 and v_2 are constants. The temporal dependence $\theta(t)$ will be specified later. Integrating (2) from nT to $(n+1)T$, with $n = 0, 1, 2, \dots$, we have $\mathbf{r}_{n+1} = M(\mathbf{r}_n, n)$, for $\mathbf{r}_n = (y_n, x_n)$, where M is a map that gives the new position \mathbf{r}_{n+1} for discrete time n . For $T = 2\pi$ we have

$$\begin{aligned} y_{n+1} &= y_n - K \sin(2\pi x_n + \theta_n) \pmod{1}, \\ x_{n+1} &= x_n + y_{n+1} \pmod{1}, \end{aligned} \quad (4)$$

where $K = v_1 v_2 T / 2\pi$, $\theta_n = \theta(t = nT)$, $\mathbf{r}_n = \mathbf{r}(t = nT)$ and $\mathbf{r}_{n+1} = \mathbf{r}[t = (n+1)T]$. In the case $\theta_n = 0$ map (4) reduces to the standard map [16]. Evaluating the determinant of map (4) we have $\det M = 1$, so M conserves the phase space area, which is derived from the incompressibility concern in (1).

In order to model mixing of the passive contaminant Φ we choose θ_n in map (4) to assume a randomic behavior in time, such as $\theta_n = 2\pi R \delta_n$ (random phase between 0 and 2π), where δ_n is a random number in the domain $[0, 1]$ and R , $0 \leq R \leq 1$, is a constant that indicates the random strength and is denominated noise parameter. In the limit case $R = 0$ we have the well known standard map [17]. Note the choice of a random function does not affect, in Eq. (1), the incompressibility of the flow, and the consequent conservative character of map (4).

The computational algorithm to obtain images of the scalar field Φ is as follows. Let $\Phi(\mathbf{r}, n)$ be the value of the Φ field at position $\mathbf{r} = \mathbf{r}_n$ and time $t = nT$. The value of $\Phi(\mathbf{r}, n)$ is obtained using the inverse iteration of the map; as Φ is constant along the trajectories, we have

$$\Phi(\mathbf{r}_n, nT) = \Phi_0(\mathbf{r}_0, 0) \quad (5)$$

for Φ_0 the initial Φ distribution, at $t = 0$.

The flux images for $N = 0$, $N = 4$, $N = 8$ and $N = 12$ iterations are shown in Fig. 1. For $N = 0$ we have the initial distribution, $\Phi_0(\mathbf{r}) = \sin(2\pi x)$. Darker regions correspond to larger initial concentration of the contaminant, N denotes particular values of n index.

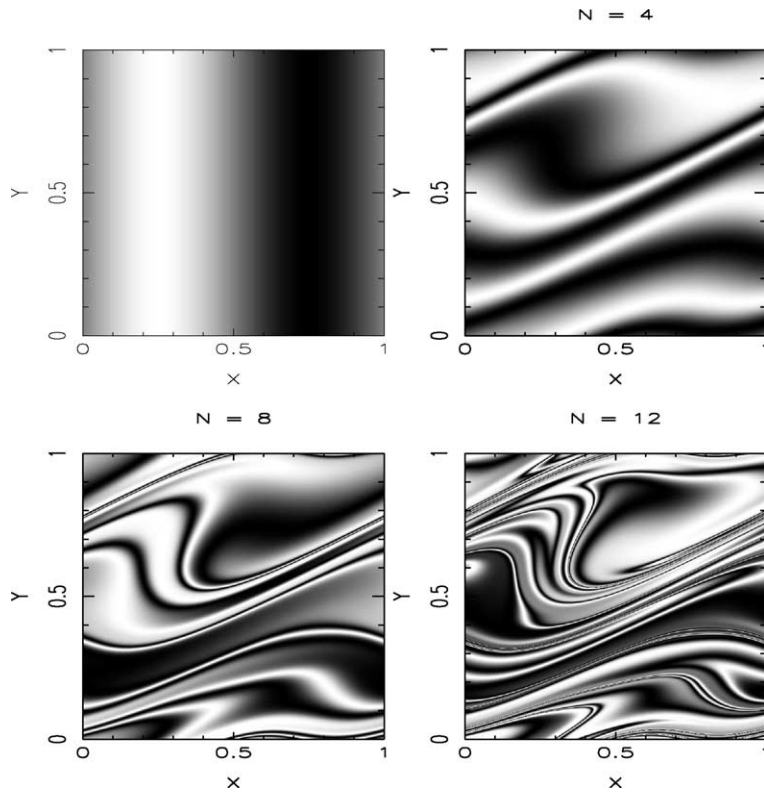


Fig. 1. Image of flux for sine-like initial scalar field (upper left), $N = 4$, $N = 8$ and $N = 12$ iterations.

3. Distribution of passive contaminant

In order to characterize the distribution properties of the concentration of the passive contaminant Φ we introduce initially the fluctuation function

$$\delta\Phi_i \equiv \Phi_i - \langle \Phi \rangle, \tag{6}$$

where the average $\langle \Phi \rangle$ is obtained over all values of the series. In fact, $\delta\Phi_i = \delta\Phi_i(\mathbf{r})$ is a local function, and i is the time/space index in time/space series. Two situations of initial concentration of contaminant, the linear-like $\Phi_0(\mathbf{r}) = 2x - 1$ and the sine-like $\Phi_0(\mathbf{r}) = \sin(2\pi x)$, are used in the work.

In Fig. 2 is plotted the histogram $P(\Phi)$, the distribution of Φ values in a spatial series for an initial linear-like Φ_0 , $K = 0.2$, the number of iterations $N = 50$, and three values of random parameter: $R = 0$ (a), $R = 0.08$ (b) and $R = 1.0$ (c). We use 10^5 values in the initial linear-like distribution taken on positions $(x_i, y_i) = (i/10^5, 0)$, $i = 1, 2, \dots, 10^5$. The points to compute $P(\Phi)$ are spread over 500 cells and their respective values are normalized by the number of points. By construction, the smoothing of $P(\Phi)$ is a measure of spacial mixing. It is concluded from the figure by visual inspection that increasing R is equivalent to increasing mixing.

For a large time of convection, $N \rightarrow \infty$, the global behaviour of Φ is determined by Φ_0 . If we consider x as a random variable, then the probability density function (p.d.f.) of any monotonic function $\Phi_0(x)$ will be given by, $f(\Phi_0) = f(x) |d\Phi_0/dx|^{-1}$ [18]. As x is concerned uniformly random distributed, then $f(x) = 1/(x\text{-range}) = 1$. Obviously the p.d.f. is related to its discretized from $P(\Phi)$ by a scale factor. For the linear Φ_0 , $f(\Phi_0) = 1/2$, a constant, which stands for a uniform distribution. For this Φ_0 the complete homogenization is attained when the particles are uniformly distributed along the full x -range, or $P(\Phi_0) = (x\text{-range})/\text{cell number} = 1/500$. In Fig. 2 we have $P(\Phi_0) \approx 0.002$, in good agreement to the predicted value.

For an initial sine-like distribution we have

$$P(\Phi_0) \sim f(\Phi_0) = \frac{1}{2\pi \cos(2\pi x)} = \frac{1}{2\pi \sqrt{1 - \Phi_0^2}}. \tag{7}$$

Fig. 3 takes time series collected at the point $(x, y) = (0, 0)$ for (a) linear-like and (b) sine-like initial distributions, $K = 0.2$, $R = 1.0$ and $N = 10^5$ iterations. In Fig. 3(a) we have an almost constant value of $P(\Phi) \approx 0.002$, as in Fig. 2, estimated for space series, while in Fig. 3(b) we observe that the generic aspect of the distribution follows the theoretical equation (7), also for space series. This result thus provides a simple numerical evidence of the ergodicity of the map (4).

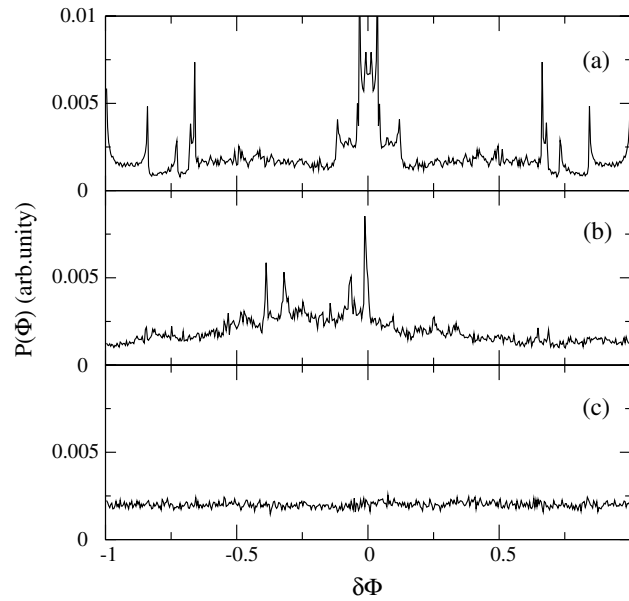


Fig. 2. Distribution $P(\Phi)$ (space series) for $K = 0.2$, $N = 50$ and $R = 0$ (a), $R = 0.08$ (b) and $R = 1$ (c).

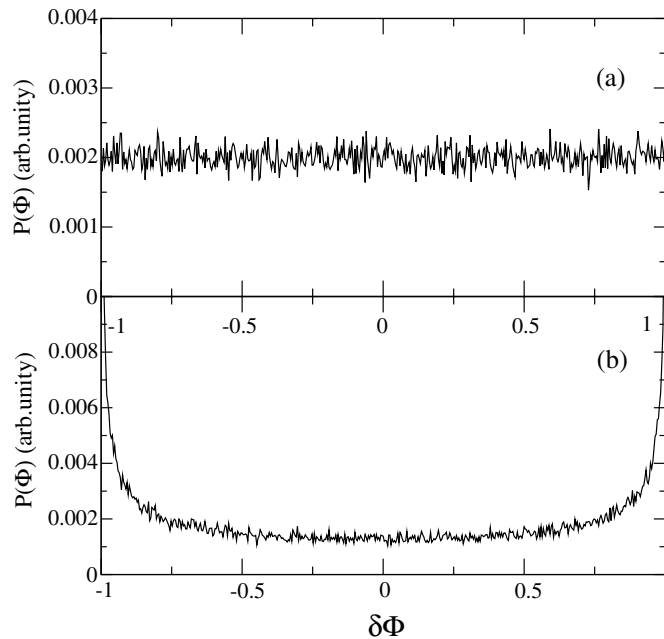


Fig. 3. Distribution $P(\Phi)$ (time series at point $(0, 0)$) for $K = 0.2$, $N = 10^5$ iterations and $R = 1$, initial linear distribution (a) and sine-like (b).

4. Folding characterization

Fig. 4 shows the dynamics of a tracing line defined by $y = 0, 0 \leq x \leq 1$ at initial time $N = 0$. For simulation we considered a discretized tracing line defined by $(x_0^{(i)}, y_0^{(i)}) = (i/N_p, 0)$, for $i = 1, 2, \dots, N_p, N_p = 3 \times 10^4$ points, $K = 0.2, R = 1.0$, and $N = 1$ (a), $N = 4$ (b), $N = 7$ (c), and $N = 10$ (d). We identify here the typical stretching and folding characterizing chaotic fluids [2]. To explore pattern convection in the fluid we analyse the behaviour of that tracing line as map dynamics takes place.

For that we introduce two quantities: the total line length at N th iteration, L_N , and the average derivative, A_N , defined by

$$A_N = \frac{1}{L_N} \int_0^{L_N} \left| \frac{dr(l)}{dl} \right| dl, \tag{8}$$

where l is the line length coordinate and $r(l) = |\mathbf{r}|$ is the modulus of the position vector on the line coordinate l . A_N describes the average modulus derivative of a line as the map M evolves and is related to the degree of deformation of the tracer line. A geometric interpretation can be realized from an illustrative example.

Fig. 5(a) shows the same line plotted in Fig. 4(a); $\mathbf{r}(l)$ is the vector position on the convected line. Fig. 5(b) presents $r(l)$ versus l for that case. Fig. 5(c) shows the derivative modulus of the precedent curve. A is then the average

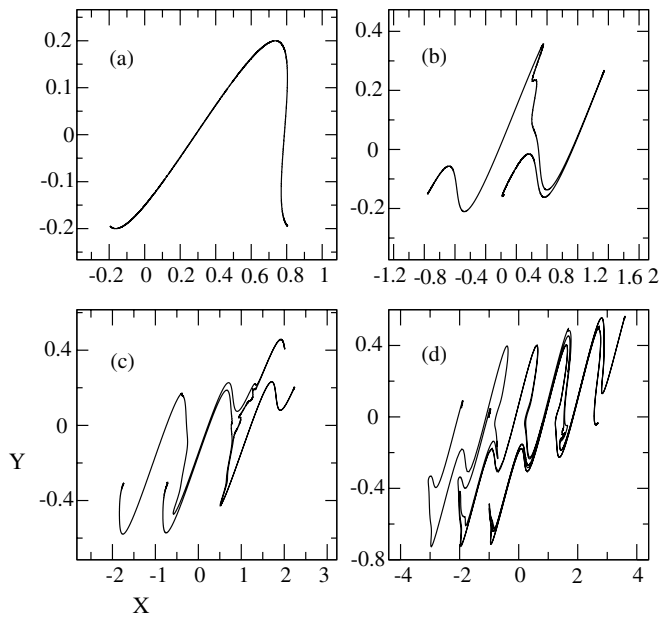


Fig. 4. The dynamics of the line for $N_p = 3 \times 10^4, K = 0.2$ and $R = 1: N = 1$ (a), $N = 4$ (b), $N = 7$ (c), and $N = 10$ (d).

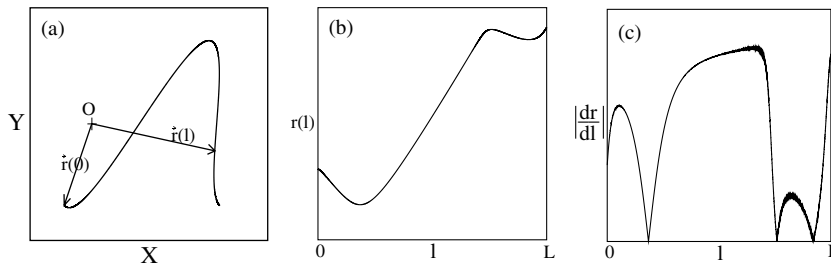


Fig. 5. Evolved tracer line (a); O is the origin of the coordinate system, r versus the tracer line length L (b); the derivative modulus of r (c).

derivative. As the integral in (8) is normalized by the length line L , since it changes at each iteration, an uniform framework is introduced for comparisons between iterations. It is important to note that the bigger the line deformation the bigger the absolute derivative values, so A_N is clearly connected to the folding due to convection. The parameter has also the advantage to require only first derivatives to be calculated.

We proceed on calculations by using the discretized form of (8). As $I_N^{(i+1)} - I_N^{(i)} \geq 0$ we have

$$A_N = \frac{1}{L_N} \sum_{i=1}^{N_p-1} \left| r_N^{(i+1)} - r_N^{(i)} \right| \tag{9}$$

and

$$L_N = \sum_{i=1}^{N_p-1} \left| \mathbf{r}_N^{(i+1)} - \mathbf{r}_N^{(i)} \right|, \tag{10}$$

where $r_N^{(i)} = |\mathbf{r}_N^{(i)}| = [(x_N^{(i)})^2 + (y_N^{(i)})^2]^{1/2}$. Expression (9) is consistent since it tends to (8) for $N_p \rightarrow \infty$.

Fig. 6 shows L_N/L_0 versus N for $K = 0.2$ (a) and L_5/L_0 versus K (b), for $N = 5$, $N_p = 10^7$ and $R = 1.0$. Note that we defined $L_0 = 1$. We presented just one simulation, additional simulations with other randomic sequences do not differ significantly. The exponential dependence of L_N , the total length of the line, versus N results from the stretching of the map M . The exponential dependence in Fig. 6(b) is qualitatively explained appealing to the limit case $R = 0$, the standard map. The linearization around the hyperbolic fixed point of period one, at $(x, y) = (0, 0)$, produces the following pair of eigenvalues [16]:

$$\lambda_{1,2} = \exp(\pm\sigma), \tag{11}$$

where $\sigma = \text{arcosh}(1 - K/2)$. Around the hyperbolic point, for each iteration, the phase space is stretched by the large eigenvalue in the direction of the unstable manifold \hat{u}_u , and contracted, in the direction of the stable manifold \hat{u}_s , by the small one. Considering that the main stretch effect in the map comes from the hyperbolic point of the period one island, for the standard map the volume element of phase space is, in the average, stretched by a factor proportional to λ_1 . As for small K the function $\text{arcosh}(1 - K/2)$ is roughly linear, the exponential behaviour in Fig. 6(b) results from the almost linear K factor in the exponent of Eq. (11).

The deviation from linear variation in Fig. 6(b) observed for $K > K_{\text{sim}} \approx 1.0$, $R = 1$, is qualitatively related to the breaking of the last KAM curve and the transition to global chaos of the standard map ($R = 0$). The best result using renormalization technique [16] including loss of stability at rational iterates of golden mean evaluates the breaking of the last KAM curve for $K_{\text{cri}} = 0.9716$.

Fig. 7 shows A_N versus N (a) for $K = 0.2$ and A_N versus K (b) for $N = 5$, in both cases $R = 1$. Three random phase sequences in (4) were considered. As L_N mainly estimates the stretching of the map, A_N , the average derivative, estimates its folding. In Fig. 7(a) A_N seems to tend to a constant for large N . In fact, integral factor in (8) scales exponentially as L_N , so any segment of tracing line should be present, at least for most time, the same folding feature. We conjecture this

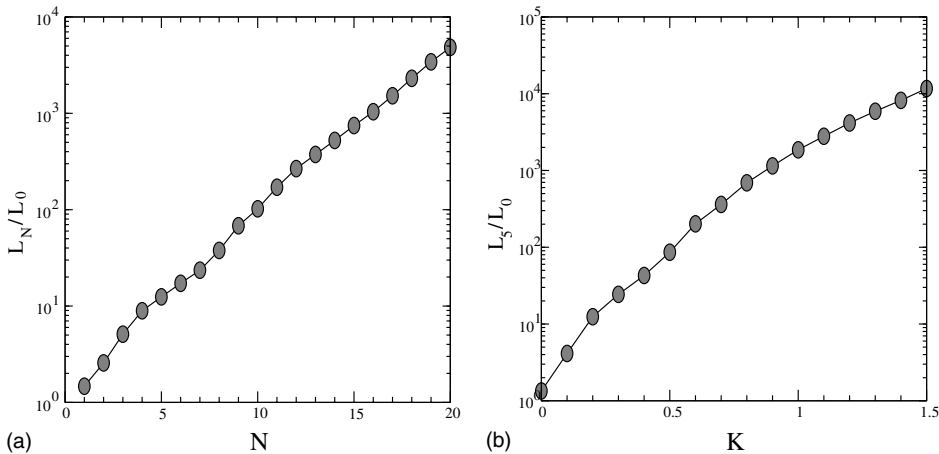


Fig. 6. L_N/L_0 versus N for $K = 0.2$ (a) and L_5/L_0 versus K for $N = 5$ (b); $R = 1$.

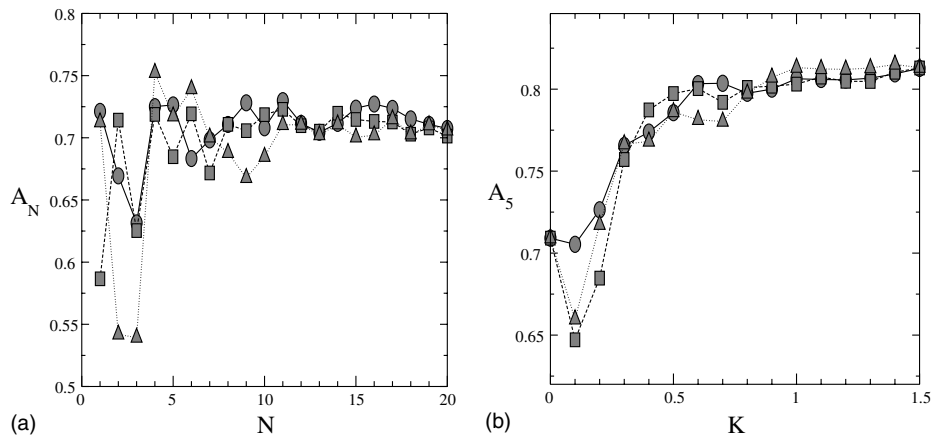


Fig. 7. A_N versus N for $K = 0.2$ (a) and A_N versus K for $N = 5$ (b), for three different random simulations; $R = 1$.

behavior is typical of all conservative chaotic fluids. In Fig. 7(b) we find the same apparent result, mainly after the $K_{\text{sim}} \approx 0.5$ value mentioned before related to the breaking of the last KAM curve in standard map.

5. Conclusion

A bidimensional chaotic fluid model described by a randomized standard map was studied. Although the map is perturbed by a randomic phase the area preserving property is not affected. Histograms of space and time series of the scalar fields depend on the initial scalar field distribution, they are predicted from the conservativity of the model and provide numerical evidence of the ergodicity of the map. The typical stretching and folding due to the chaotic convection were quantified by the defined parameters L_N , the total length of the iterated tracer line, and A_N , the average derivative of the iterated tracer line. A_N is a new tool to characterize the stretching of a map and provides a direct way to quantify folding features in the studied chaotic flux. It seems to tend to a constant in the studied model. This behavior is a consequence of stretching and folding in conservative flux and should be verified in the Lagrangian transport of other conservative systems.

Acknowledgements

This work was supported by Fundação de Amparo à Pesquisa do Estado de São Paulo, grant 1995/08813-0.

References

- [1] Aref H. Stirring by chaotic advection. *J Fluid Mech* 1984;143:1–21.
- [2] Ott E. *Chaos in dynamical systems*. Cambridge: Cambridge University Press; 1993.
- [3] Ottino JM. *The kinematics of mixing: stretching, chaos and transport*. Cambridge: Cambridge University Press; 1989.
- [4] Crisanti A, Falcioni M, Vulpiani A, Paladin G. Lagrangian chaos—transport, mixing and diffusion in fluids. *Riv del Nuovo Cimen* 1991;14:1–80.
- [5] Toroczkai Z, Károlyi G, Pentek A, Tél T, Grebogi C. Advection of active particles in open chaotic flows. *Phys Rev Lett* 1998;80:500–3.
- [6] Aref H. Stochastic particle motion in laminar flows. *Phys Fluids A* 1991;3:1009–16.
- [7] Chaiken J, Chu CK, Tabor M, Tran QM. Lagrangian turbulence and spatial complexity in a Stokes-flow. *Phys Fluids* 1987;30:687–94.
- [8] Dombre T, Frish U, Greene JM, Hénon M, Mehr A, Soward AM. Chaotic streamlines in the ABC flow. *J Fluid Mech* 1986;167:353–91.
- [9] Doxas I, Horton W, Berk HL. Stochastic diffusion in 2-dimensional periodic flows. *Phys Fluids A* 1990;2:1906–9.
- [10] Solomon TH, Gollub JP. Passive transport in time-dependent Rayleigh–Bénard convection. *Phys Fluids* 1988;31:1372–9.
- [11] del-Castillo-Negrete D. Self-consistent chaotic transport in fluids and plasmas. *Chaos* 2000;10:75–88.

- [12] Városi F, Antonsen Jr TM, Ott E. The spectrum of fractal dimensions of passively convected scalar gradients in chaotic fluid flows. *Phys Fluids A* 1991;3:1017–28.
- [13] Yu L, Ott E, Chen Q. Fractal distribution of floaters on a fluid surface and the transition to chaos for random maps. *Physica D* 1991;53:102–24.
- [14] Toussaint V, Carrière P, Raynal F. A numerical Eulerian approach to mixing by chaotic advection. *Phys Fluids* 1995;7:2587–600.
- [15] Romeiras FJ, Grebogi C, Ott E. Multifractal properties of snapshot attractors of random maps. *Phys Rev A* 1990;41:784–99.
- [16] Lichtenberg AJ, Leiberman MA. *Regular and chaotic motion*. 2nd ed. Berlin: Springer-Verlag; 1992.
- [17] Chirikov BV. A universal instability of many-dimensional oscillator systems. *Phys Rep* 1979;52:265–379.
- [18] Papoulis A. *Probability, random variables, and stochastic processes*. New York: McGraw-Hill; 1965.